Available online at www.sciencedirect.com
ScienceDirect
Journal of Nuclear Materials 372 (2008) 405–415
journal of nuclear materials
www.elsevier.com/locate/jnucmat

Thermal diffusion of iodine in UO_2 and UO_{2+x}

Madiba Saidy [a,*], William H. Hocking [a], Jozef F. Mouris [a], Philippe Garcia [b], Gaëlle Carlot [b], Bertrand Pasquet [b]

[a] Atomic Energy of Canada Limited (AECL), Chalk River Laboratories (CRL), Chalk River, Ontario, Canada K0J 1J0
[b] Commissariat à l'Energie Atomique (CEA), Centre de Cadarache, CEA/Cad/DEC, Bâts 130 & 316, 13108 St-Paul-lez-Durance, France

Received 24 October 2006; accepted 20 March 2007

Abstract

An inter-laboratory comparison has provided enhanced confidence in a novel out-reactor method that has been developed for investigating the migration behaviour of fission products in oxide nuclear fuels. Changes in the distribution of ion-implanted fission products caused by thermal annealing or radiation damage are precisely determined using high-performance secondary ion mass spectrometry. Accurate measurements of iodine thermal diffusion in stoichiometric UO_2 – on single-crystal as well as polycrystalline ceramic samples over the temperature range 1200–1650 °C for periods ranging from 1 h to 24 h – have yielded a refined Arrhenius relationship. An increase in both the solubility and diffusion rate of iodine by two orders of magnitude compared to stoichiometric fuel was found when the annealing was performed at 1400 °C under slightly oxidizing conditions sufficient to achieve a nominal O/U ratio of 2.02. These effects are consistent with the increase in the population of uranium lattice vacancies predicted by a thermodynamic model for the defect structure of UO_{2+x}.

PACS: 66.30.−h; 66.30.Jt; 82.80.Ms; 85.40. Ry

1. Introduction

Segregation of fission products with low solubility in uranium dioxide is a determining factor for performance and safety throughout the nuclear fuel cycle [1–4]. At high burnup, release of inert fission gases from the fuel matrix can be sufficient to cause overpressure strain of the fuel sheath (cladding). Several volatile fission products, most notably iodine, have been implicated in fuel failures caused by stress-corrosion cracking (SCC) of the zirconium alloy sheath [5]. Moreover, release of radionuclides from defected fuel elements during reactor operation contributes to activity transport and occupational radiation exposures [3]. Accumulation of segregated fission products at the fuel grain boundaries and at the fuel–sheath interface also enhances the potential for release of radioactivity to the environment in the event of an accident and from spent fuel during storage or after permanent disposal [2–4]. Despite the significant progress that has been achieved over the past half century in understanding the properties of oxide nuclear fuels, there is still considerable uncertainty in the migration behaviour of several key fission products [1–4].

The first stage, and normally the rate-determining step, in segregation and release of fission products is diffusion to the fuel grain boundaries [3]. During reactor operation, three distinct regimes have been recognized, which are dependent upon whether the two processes necessary for diffusion – formation of vacancies and migration of vacancies – are predominantly controlled by thermal activation or radiation [6]. Migration of lattice atoms and fission products has been shown to be athermal and directly proportional to the fission rate at temperatures below ~1000 K. This radiation-induced diffusion (RID) has been interpreted as resulting from transient thermal-spike and pressure-gradient effects that occur along fission tracks

* Corresponding author. Tel.: +1 613 584 3311; fax: +1 613 584 8214.
E-mail address: saidym@aecl.ca (M. Saidy).

0022-3115/$ - see front matter © 2007 Elsevier B.V. All rights reserved.
doi:10.1016/j.jnucmat.2007.03.272

[6–8]. At higher temperatures, fission products can move by thermally activated jumps between lattice vacancies created by radiation damage – providing radiation-enhanced diffusion (RED) [6,8]. The formation of lattice vacancies, as well as the movement of fission products between them, becomes thermally controlled above ~1600 K, although thermal diffusion (TD) is usually fast enough to allow significant segregation to the fuel grain boundaries only at yet higher temperatures [6,9]. Because the concentration of uranium lattice vacancies in UO_{2+x} increases rapidly as a function of x, any appreciable degree of hyperstoichiometry would provide a greatly enhanced population of sites that can be occupied by migrating fission products, in both the RED and TD regimes [9–12]. If the solubility limit of a particular fission product in the fuel matrix is exceeded, precipitation as microscopic intragranular particles or bubbles may occur. These sites can act as effective traps or sinks for that fission product, thereby inhibiting its migration through the fuel matrix, unless they are disrupted by fission spikes or displacement cascades – radiation-induced re-solution [13,14].

Information on the diffusion of fission products in oxide nuclear fuels has been derived historically from measurements of the release of radiotracers; however, the correct interpretation of such data can be very difficult and results spanning many orders of magnitude have been reported [6,9,10,15–19]. Furthermore, the Booth model, which has been used to analyze the release data, yields an effective diffusion coefficient, D/a^2, where a is the radius of a hypothetical sphere equivalent to the diffusion volume [20]. For experiments on polycrystalline ceramic fuel samples, evaluating the appropriate value of this sphere radius introduces considerable further uncertainty into the final result [15,18,21]. Direct measurement of the diffusive spreading of a concentrated source, such as a deposited film, is generally recognized as the only reliable approach for determining diffusion coefficients [16,17,19,22]. Over the past few years, an improved method for investigating the migration behaviour of fission products in oxide nuclear fuels has been developed [23,24]. Tailored fission-product distributions are first created in the near-surface region of polished wafers by ion implantation; subsequently, changes arising from thermal annealing or radiation damage are precisely determined by depth profiling using high-performance secondary ion mass spectrometry (SIMS) [23,24].

A joint program to investigate the migration behaviour of fission products in fuel using the ion-implantation/SIMS method has been undertaken by Atomic Energy of Canada Limited, Chalk River Laboratories (hereafter CRL) and Commissariat à l'Énergie Atomique, Cadarache, France (hereafter CEA). The objective of this collaboration is not only to leverage the resources and capabilities of the individual organizations but also to provide further confirmation of the results through comparison of different analytical procedures. Recent studies of the solubility and thermal diffusion of iodine in stoichiometric UO_2 and hyperstoichiometric UO_{2+x} (in the form of single crystals as well as polycrystalline ceramic) are the subject of this paper.

2. Experimental procedures

A majority of the experiments were performed using polycrystalline ceramic UO_2 wafers ~2 mm thick, although a few measurements were also made on thin slices cut from a UO_2 single-crystal for comparison. The polycrystalline samples prepared at CRL had been sintered to ~97% of the theoretical density, with polygonal, equiaxed grains mainly 5–15 μm in size, whereas all of the samples prepared at CEA had achieved ~98% of the theoretical density, with grain sizes in the 5–20 μm range. Mechanical damage created by polishing [25] one face of each sample to a 0.05 μm finish was removed by annealing at 1500 °C in Ar–4%H_2 (at CRL) or at 1400 °C in Ar–5%H_2 (at CEA). Tailored concentration profiles of iodine were then introduced just below the surface of the polished face by ion implantation; near-Gaussian distributions of ^{127}I, with mean projected ranges from ~20 nm up to ~150 nm, were created by employing different ion-implantation energies between 100 keV and 930 keV. The implantations were performed using tandem accelerators operated by Interface Science Western at the University of Western Ontario (UWO) in Canada and the Institut de Physique Nucléaire de Lyon in France. A uniform concentration was ensured by rastering a focussed ion beam across an area larger than the wafer, which could be subsequently divided into two or more pieces to obtain identical duplicate samples. Different wafers were implanted to iodine fluences spanning four orders of magnitude, from 1×10^{15} ions/m^2 to 1×10^{19} ions/m^2.

Diffusive spreading of the implanted-iodine layer was induced by annealing at peak temperatures between 1180 °C and 1650 °C for periods ranging from 1 h to 24 h, either in a high-density alumina tube furnace (at CRL) or in a molybdenum sintering furnace (CEA). A type B thermocouple was used to monitor the *in-situ* temperature. The oxygen potential within the furnace was normally controlled by a flowing gas mixture of Ar–4%H_2, which should preserve a nearly stoichiometric UO_2 composition [18]. A few thermal anneals were intentionally performed under slightly oxidizing conditions to achieve a nominal O/U ratio of either 2.01 or 2.02; for this purpose, a coulometric titration system was used to control the oxygen potential within the alumina tube furnace (at CRL) [26]. A gas mixture of 1300 ppm H_2 in argon was passed through a combination electrolysis and measurement cell, where a controlled amount of oxygen was added to it, before entering the tube furnace. After being exposed to the sample at high temperature, the gas mixture then passed through a second electrolysis and measurement cell where the amount of oxygen absorbed by the ion-implanted sample was measured. In order to ensure that the desired O/U ratio was achieved, the system was calibrated using a standard UO_2 sample, of a similar weight

and shape to the ion-implanted sample, before each experiment [26].

The iodine distributions within both diffused and as-implanted samples were measured by secondary ion mass spectrometry using Cameca IMS 6f SIMS instruments at three different locations: at CRL and CEA, where the instruments have been customized for the safe handling of radioactive materials and irradiated fuels respectively [23,27], and at the Centre d'Informatique et de Géologie (CIG) of the Ecole des Mines in Fontainebleau, France. A double-focussing magnetic-sector mass spectrometer provides high throughput for secondary ions, which are detected with an electron multiplier operated in the single-ion counting mode. The pressure inside the sample chamber was $<10^{-7}$ Pa during the analyzes. At CRL, iodine was detected as I^- and a Cs^+ primary-ion beam was used to enhance the yield of negative secondary ions [28]. A focussed 10 keV Cs^+ beam, with a diameter of ~30 μm and a current of ~25 nA to ~65 nA, was rastered over an area of 250 μm by 250 μm on the sample surface. Secondary ions were efficiently collected, using a 5 kV extraction field, from a smaller region (60–100 μm in size) located in the centre of the sputtered area in order to minimize crater-edge effects; comparable results were obtained using both optical and electronic (raster) gating [28]. At CEA and CIG, iodine was also detected as I^-, but a 12.5 keV O_2^+ primary beam was used for sputtering. In this case, the focussed primary beam, with a current of ~300 nA, was rastered over a 150 μm by 150 μm area on the sample and the signal was extracted from a ~60 μm region (optical gating).

The depth scale for every profile recorded at CRL was subsequently determined by measuring the depth of the sputtered crater using a Tencor Alpha-Step 500 stylus profilometer, which was routinely calibrated against a thin step-height standard (450 ± 3 nm) purchased from VLSI Standards Inc. Significant roughness developed in the bottom of craters sputtered in polycrystalline samples, because of differences in sputtering rates for the various UO_2 grain orientations [23]. An average crater depth was then derived from eight line scans recorded across the central region of each crater in two orthogonal directions; since between 50 and 100 grains are included in the analysis area, the effects of different grain orientations should be largely averaged out. The single-crystal samples invariably yielded craters with a smooth, flat bottom, which allowed their depth scale to be accurately determined. Calibration of the depth scale on the profiles recorded at CEA or CIG was based upon SRIM calculations [29], which can be used to obtain a good estimate of the mean projected range of the iodine atoms implanted into the sample. The sputtering rate, which is assumed to be constant throughout the experiment, was then obtained by dividing the mean projected range by the sputter time required to reach the maximum iodine concentration in the profile.

Depth profiles were always recorded in pairs – one from a diffused sample and the other from its as-implanted duplicate – under identical instrument operating conditions. In a few cases, both reference and annealed samples were coated with a very thin film of gold before the SIMS analysis to mitigate potential surface charging. The concentration scale for the as-implanted sample could be determined from the integrated area under the profile and the known implantation fluence [28]. A relative sensitivity factor (RSF) for I^- normalized to a matrix species could then be derived for these analytical conditions [28]. Finally, application of this RSF to the profile for the 'diffused' sample allowed its concentration scale to be calibrated – independent of any loss due to volatilization from the surface. Generally good agreement was obtained using U, UO and UO_2 as the matrix species for the RSF normalization.

Thermal annealing experiments were performed under reducing conditions on ceramic UO_2 wafers that had been ion-implanted with ^{127}I at 800 keV to a low fluence (1×10^{15} ions/m^2) by CEA at five different temperatures for various periods as follows: 1180 °C for 8 h, 1280 °C for 24 h, 1370 °C for 4 h and 7 h, 1450 °C for 3 h and 5 h, and 1550 °C for 1 h and 2 h. Duplicate samples prepared in France were sent to CRL for analysis to facilitate an inter-laboratory comparison of results obtained using different instruments and analytical techniques. Additional samples (both ceramic and single-crystal UO_2) were prepared and analyzed at CRL to complement the above suite of experiments as follows: implants of ^{127}I at 100 keV to 1×10^{15} ions/m^2 were annealed at 1200 °C for 24 h and at 1300 °C for 5 h under reducing conditions; an implant of ^{127}I at 930 keV to 1×10^{17} ions/m^2 was annealed at 1465 °C for 2 h under reducing conditions; implants of ^{127}I at 440 keV to 1×10^{17} ions/m^2 or 1×10^{19} ions/m^2 were annealed at 1200 °C or 1400 °C for 2.5 h under slightly oxidizing conditions.

Accurate diffusion coefficients have been derived from the measured diffusive spreading of the iodine distributions by numerically solving the one-dimensional partial differential equation that represents Fick's second law using the *Mathematica* software package (from Wolfram Research, Champaign, Illinois) [24,30–32]. An initial estimate of the diffusion coefficient for each experiment was normally obtained using a relationship derived by applying random-walk theory to the individual jumps over atomic distances [33]:

$$D = (\langle X \rangle)^2/(2 \cdot t), \tag{1}$$

where D is the diffusion coefficient, $\langle X \rangle$ is the mean diffusive spreading and t is the annealing time (at peak temperature). These estimates provided a useful starting point for the detailed numerical analysis of the entire profile and typically agreed reasonably well with the final result.

Aside from the differences in the analytical techniques (SIMS operating conditions and depth-scale calibration) between CRL and CEA described above, different approaches were also taken to derive diffusion coefficients from the numerical analysis of the altered profiles. At

CRL, the numerical analysis was optimized to provide the best overall match to all of the available data for each experiment, yielding a single value for the diffusion coefficient. Conversely, at CEA, each pair of reference and annealed profiles was analyzed separately and the results from multiple analyzes (for the same experiment) were then combined to obtain an average value for the diffusion coefficient with a standard deviation.

3. Results and discussion

3.1. Thermal diffusion of iodine in stoichiometric UO_2

The effects of thermal annealing at 1180 °C for 8 h on the depth distribution of iodine ion-implanted in polycrystalline UO_2 at 800 keV to a fluence of 1×10^{15} ions/m^2 are illustrated in Fig. 1 (sample prepared (implanted and annealed) at CEA but analyzed at CRL). Because diffusion of iodine under these conditions is extremely slow [24], this represents a severe test of the sensitivity of the method. The maximum iodine concentration at the peak of the as-implanted reference profile (about 6×10^{21} atoms/m^3) is well below the $\sim 10^{22}$ atoms/m^3 threshold level previously identified for defect trapping [24]. Duplicate profiles recorded from the as-implanted as well as the annealed samples demonstrate excellent reproducibility except in the tail of the annealed distribution, and provide clear evidence of a small degree of iodine migration into the bulk matrix as well as some reduction in the peak concentration. A simple diffusion analysis, with a constant diffusion coefficient of 3.5×10^{-20} m^2/s over the entire depth (depicted by the solid curve), provided a reasonable fit to the altered distribution.

The impact of thermal annealing at 1200 °C for 24 h on the depth distribution of iodine ion-implanted in polycrystalline UO_2 at 100 keV to a fluence of 1×10^{15} ions/m^2 is illustrated in Fig. 2 (sample prepared and analyzed at CRL); the longer annealing time and shallower initial distribution have caused a larger relative change in the iodine distribution here. A simple diffusion analysis, with a constant diffusion coefficient of 9.3×10^{-21} m^2/s, which is almost a factor of four smaller than the value derived from Fig. 1, provided the best fit to the altered distribution. Deviations between the measured and calculated iodine distributions in the tail of the profiles in both figures, which are emphasized by the logarithmic concentration scale, could arise from artefacts of the SIMS depth profiling and/or faster migration along grain boundaries. Migration of iodine at shallow depths, near the peak in the initial distribution, might also be influenced by trapping effects or radiation damage created during the implantation [24].

The migration of iodine (ion-implanted in polycrystalline UO_2 at 800 keV to a fluence of 1×10^{15} ions/m^2) caused by a 24 h anneal at 1280 °C is illustrated in Fig. 3

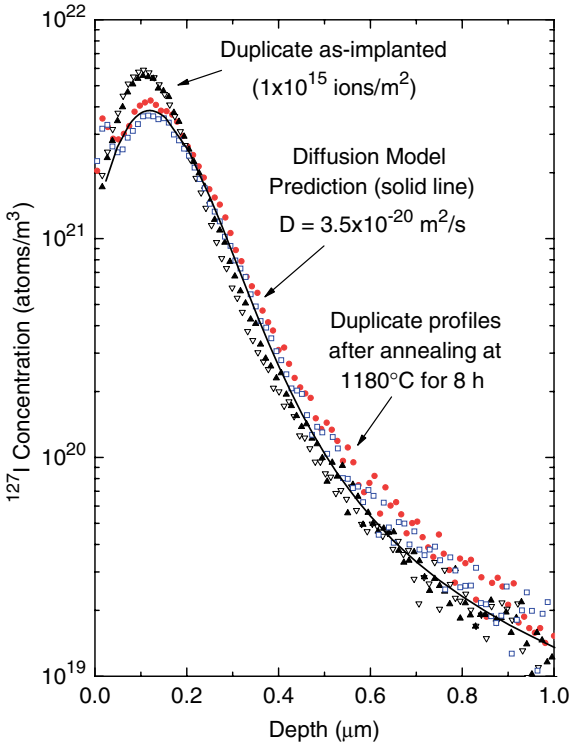

Fig. 1. Depth profiles of ^{127}I as-implanted in polycrystalline UO_2 at 800 keV to a fluence of 1×10^{15} ions/m^2 and after a thermal anneal at 1180 °C for 8 h under reducing conditions (sample prepared (implanted and annealed) at CEA but analyzed at CRL). The calculated (model-prediction) distribution is indicated by the solid line.

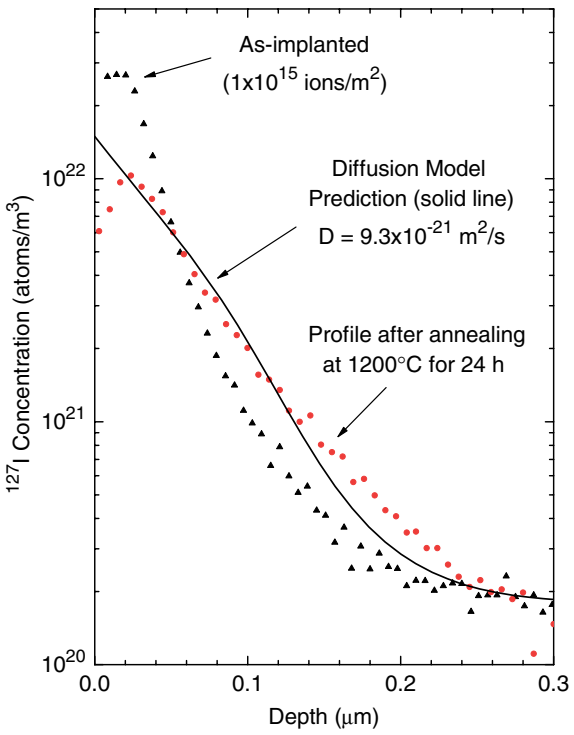

Fig. 2. Depth profile of ^{127}I as-implanted in polycrystalline UO_2 at 100 keV to a fluence of 1×10^{15} ions/m^2 and after a thermal anneal at 1200 °C for 24 h under reducing conditions (sample prepared and analyzed at CRL). The calculated (model-prediction) distribution is indicated by the solid line.

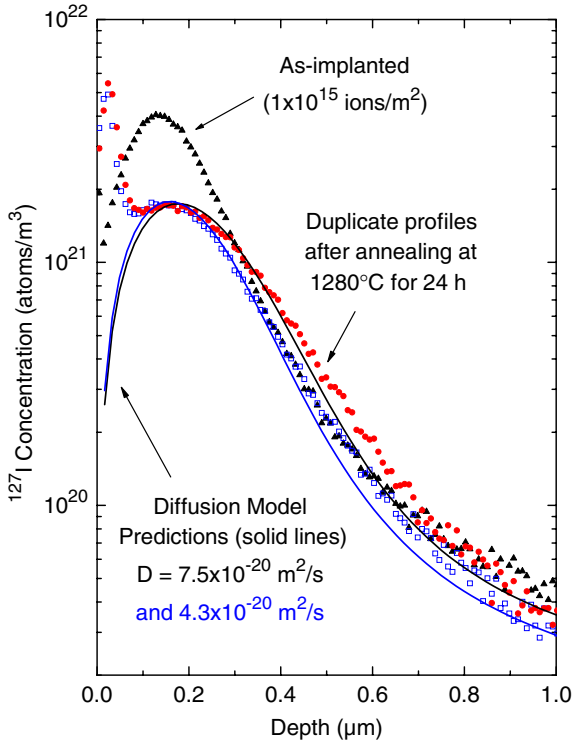

Fig. 3. Depth profile of ^{127}I as-implanted in polycrystalline UO_2 at 800 keV to a fluence of 1×10^{15} ions/m^2 and after a thermal anneal at 1280 °C for 24 h under reducing conditions (sample prepared and analyzed at CEA). Model calculations are depicted as solid lines.

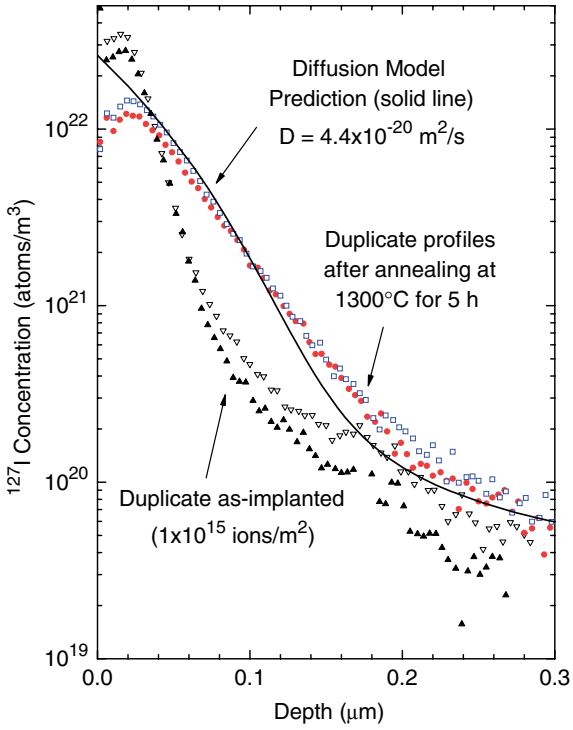

Fig. 4. Depth profiles of ^{127}I as-implanted in a UO_2 single-crystal at 100 keV to a fluence of 1×10^{15} ions/m^2 and after a thermal anneal at 1300 °C for 5 h under reducing conditions (sample prepared and analyzed at CRL). The calculated (model-prediction) distribution is indicated by the solid line.

for a sample prepared and analyzed at CEA (see Section 2 for differences in analytical procedures from CRL). Representative duplicate profiles of the annealed sample are displayed here, together with the corresponding best-fit calculations, and one as-implanted reference profile. An average diffusion coefficient of $(6.8 \pm 5) \times 10^{-20}$ m^2/s was derived from all of the data collected for this experiment (multiple analyzes combined as described above).

The impact of thermal annealing at 1300 °C for 5 h on the distribution of iodine ion-implanted in a UO_2 single-crystal at 100 keV to a fluence of 1×10^{15} ions/m^2 is shown in Fig. 4 (sample prepared and analyzed at CRL). A simple diffusion analysis, with a constant diffusion coefficient of 4.4×10^{-20} m^2/s, again provided a reasonable fit to the altered distribution (aside from the deviations at the leading and trailing ends as discussed above). Comparison of Fig. 4 with Fig. 3 further illustrates the potential advantage of using shallower implants for measuring slow diffusion at relatively low temperatures. Nonetheless, the diffusion coefficients derived for iodine lattice migration in polycrystalline UO_2 at 1280 °C (above) and in single-crystal UO_2 at 1300 °C (here) agree within the estimated uncertainty in the former.

The impact of thermal annealing at 1370 °C for 7 h on the distribution of iodine ion-implanted in polycrystalline UO_2 at 800 keV to a fluence of 1×10^{15} ions/m^2 is shown in Fig. 5 (sample prepared at CEA but analyzed at CRL). As expected, the changes in the depth distribution of iodine are more pronounced here than those observed at the lower temperatures above (compare Figs. 1–4 with Fig. 5). A simple diffusion analysis, with a constant diffusion coefficient of 2.8×10^{-19} m^2/s, again provided a reasonable fit to the key portion of the altered distribution. Selected results from another experiment performed on a duplicate sample at the same temperature (1370 °C) but for a shorter period (4 h) are displayed in Fig. 6 (sample prepared and analyzed at CEA). The average diffusion coefficient derived from combined analyzes of multiple depth profiles, $(3.7 \pm 1) \times 10^{-19}$ m^2/s, agrees with the preceding measurement (within the estimated uncertainty). Previous experiments on single-crystal and polycrystalline UO_2 ion-implanted with iodine to the same fluence and annealed at 1400 °C under reducing conditions have yielded diffusion coefficients in the range $(1.7–3.3) \times 10^{-19}$ m^2/s [24,30]. The internal consistency of all of these measurements, despite the many differences in the experimental procedures, provides enhanced confidence in the overall reliability of the method. Furthermore, the present results are also entirely compatible with diffusion coefficients derived from in-reactor measurements of iodine release from small UO_2 single crystals at 1400 °C under reducing conditions [6].

Significant migration of iodine, which had been ion-implanted in polycrystalline UO_2 at 800 keV to a fluence of 1×10^{15} ions/m^2, after thermal annealing at 1450 °C for 5 h is shown in Fig. 7 (sample prepared at CEA but

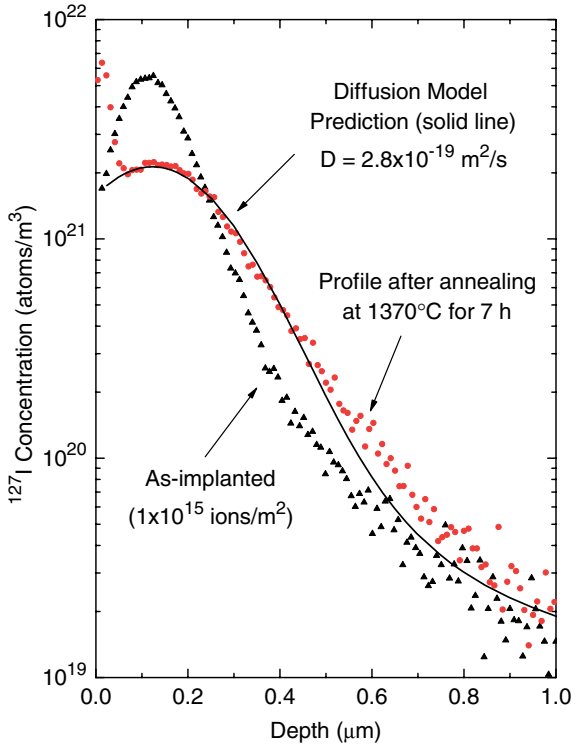

Fig. 5. Depth profiles of ^{127}I as-implanted in polycrystalline UO_2 at 800 keV to a fluence of 1×10^{15} ions/m^2 and after a thermal anneal at 1370 °C for 7 h under reducing conditions (sample prepared at CEA but analyzed at CRL). The calculated (model-prediction) distribution is indicated by the solid line.

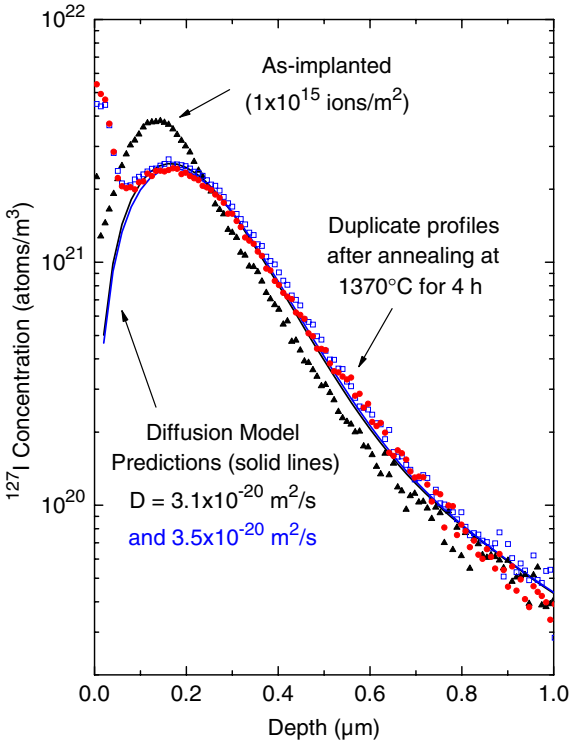

Fig. 6. Depth profiles of ^{127}I as-implanted in polycrystalline UO_2 at 800 keV to a fluence of 1×10^{15} ions/m^2 and after a thermal anneal at 1370 °C for 4 h under reducing conditions (sample prepared and analyzed at CEA). Model calculations are depicted as solid lines.

analyzed at CRL). Three profiles recorded from the annealed sample again demonstrate excellent reproducibility, whereas all of the as-implanted reference profiles were virtually superimposed (only one shown in Fig. 7). The diffusion coefficient derived from these data, 1.2×10^{-18} m^2/s, is about a factor of four greater than the values obtained above at 1370 °C, which is qualitatively consistent with the expected temperature dependence [24]. Essentially the same result was obtained from a duplicate experiment conducted entirely by CEA using a shorter annealing time of 3 h at 1450 °C – an average diffusion coefficient of $(1.1 \pm 0.2) \times 10^{-18}$ m^2/s was determined from multiple analyzes.

As illustrated in Fig. 8, even more pronounced diffusive spreading of iodine (ion-implanted in polycrystalline UO_2 at 800 keV to a fluence of 1×10^{15} ions/m^2) was caused by a thermal anneal at 1550 °C for 2 h (sample prepared at CEA but analyzed at CRL). A simple diffusion analysis, with a constant diffusion coefficient of 4.3×10^{-18} m^2/s, provided a reasonable fit to the altered distribution over the entire profile, except right near the surface. For comparison, an average diffusion coefficient of $(4.6 \pm 1.2) \times 10^{-18}$ m^2/s was derived from multiple analyzes of a duplicate experiment in which the sample was annealed for only 1 h at 1550 °C (sample preparation and analysis at CEA). The increase in the measured diffusion coefficients between 1450 °C and 1550 °C is again qualitatively consistent with the expected temperature dependence [24].

All of the samples that were thermally annealed at CEA, regardless of the analysis conditions (I^-/Cs^+ versus I^-/O_2^+), show an apparent accumulation of excess iodine right at the surface. The magnitude of this effect appears to increase with the anneal temperature (most pronounced in Fig. 8 and only just evident in Fig. 1). A similar behaviour has not been found for any of the samples prepared at CRL – including previous high-temperature anneals of deeper implants (at 440 keV and 900 keV) [24,30] as well as the results presented in Figs. 2 and 4. These observations suggest that subtle differences in the conditions during the thermal annealing could influence the release of iodine from the surface of the sample. The general agreement between the various measurements of the diffusion coefficient at 1370 °C and 1400 °C (above) indicates that there was negligible impact on migration of iodine into the matrix (in this temperature range). Conversely, the values that were previously determined for the iodine diffusion coefficient at 1520 °C (6.3×10^{-19} m^2/s) and 1650 °C (5.0×10^{-18} m^2/s) from polycrystalline UO_2 samples annealed at CRL [24,30] fall slightly below the trend established by the higher temperature measurements above (on samples annealed at CEA). Whether these discrepancies are a direct consequence of the apparent differences in the iodine concentration at the surface or simply reflect the overall precision of the method has not been estab-

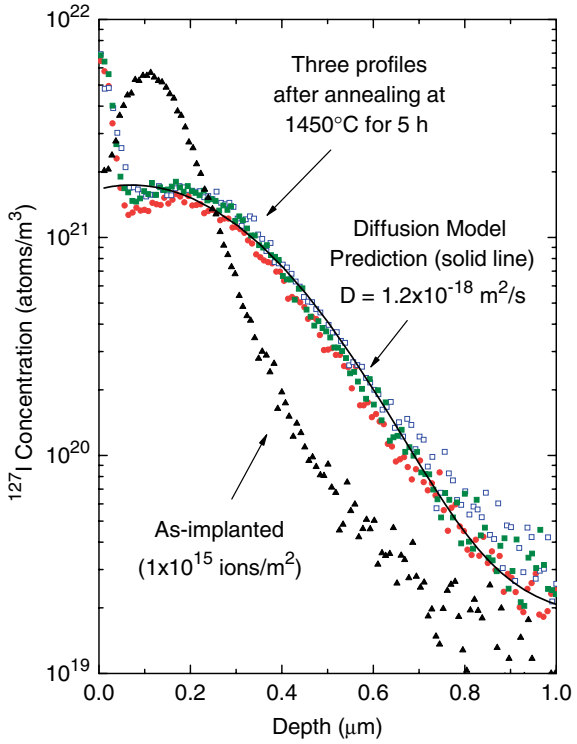

Fig. 7. Depth profiles of ^{127}I as-implanted in polycrystalline UO_2 at 800 keV to a fluence of 1×10^{15} ions/m^2 and after a thermal anneal at 1450 °C for 5 h under reducing conditions (sample prepared at CEA but analyzed at CRL). The calculated (model-prediction) distribution is indicated by the solid line.

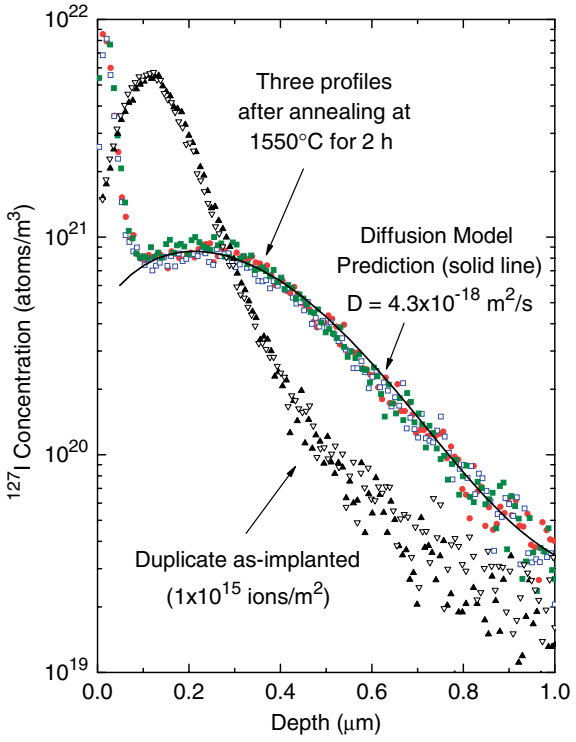

Fig. 8. Depth profiles of ^{127}I as-implanted in polycrystalline UO_2 at 800 keV to a fluence of 1×10^{15} ions/m^2 and after a thermal anneal at 1550 °C for 2 h under reducing conditions (sample prepared at CEA but analyzed at CRL). The calculated (model-prediction) distribution is indicated by the solid line.

lished; further studies that might resolve this issue seem warranted.

The more limited data from previous experiments (samples prepared and analyzed at CRL) were just sufficient to derive an Arrhenius relationship for iodine thermal diffusion in UO_2 as follows [30]:

$$D(\mathrm{m}^2/\mathrm{s}) = 4.75 \times 10^{-9}\ \mathrm{e}^{-3.44\ \mathrm{eV}/kT}, \quad (2)$$

where k is the Boltzmann constant and T is the absolute temperature. This relationship has been graphically depicted in Fig. 9, together with the previous data (red and black points) used to derive it and the in-reactor release measurements on small UO_2 single crystals (blue points) discussed above [6]. Extensive out-reactor measurements of fission-gas release from irradiated-fuel samples have yielded Arrhenius relationships that span about five orders of magnitude roughly centred on Eq. (2) [9,16,30]. A new Arrhenius relationship for iodine diffusion in stoichiometric UO_2, which is also shown graphically in Fig. 9, was obtained from the best fit to all of the existing data derived from ion-implantation experiments (except that in Fig. 1) as follows:

$$D(\mathrm{m}^2/\mathrm{s}) = 2.04 \times 10^{-8}\mathrm{e}^{-3.6\,\mathrm{eV}/kT}. \quad (3)$$

Symbols for the new results in Fig. 9 are colour-coded purple (sample prepared and analyzed by CEA), green (sample prepared by CEA but analyzed at CRL) and orange or gray (sample prepared and analyzed at CRL), whereas the older measurements (red, black and blue) were identified above. The diffusion coefficient derived from the shallow (100 keV) implant annealed at 1200 °C (solid orange diamond) is clearly in much better agreement with the higher temperature measurements (both new and old) than that obtained from the deeper (800 keV) implant annealed at 1180 °C (open green symbol); whether this reflects better measurement precision for the shallow implant at low temperatures or just an aberration in one experiment near the limit of the method remains to be confirmed.

After submission of the manuscript, an additional experiment was performed on a polycrystalline UO_2 wafer (ion-implanted with iodine at 900 keV to a fluence of 1×10^{15} ions/m^2) that provides further confirmation of the results presented above. The sample was annealed at 1700 °C for 2.5 h in a single-crystal alumina furnace tube under flowing Ar–4%H_2 and the composition of the effluent gas was monitored throughout by coulometric titration to confirm that there had been no change in the stoichiometry. A good fit to the entire diffused profile was obtained with a constant diffusion coefficient of 1.7×10^{-17} m^2/s, which has been depicted in Fig. 9 by a solid orange circle. This point is in excellent agreement with the solid blue line, despite the fact that it was not included in the analysis used to derive Eq. (3).

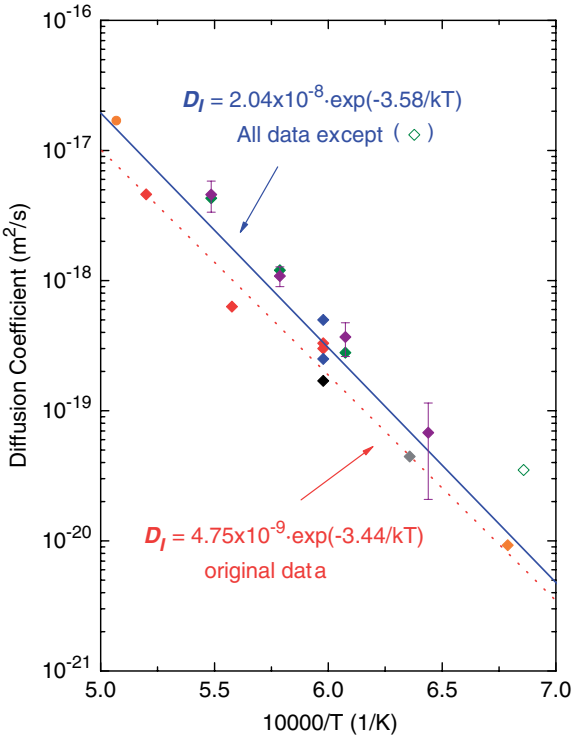

Fig. 9. Arrhenius plot of thermal diffusion coefficients determined for iodine: red and black symbols for previous measurements (at CRL) on polycrystalline and single-crystal UO_2 samples respectively, green symbols for polycrystalline UO_2 samples prepared at CEA (open green symbol corresponds to sample annealed at 1180 °C for 8 h) and analyzed at CRL; purple symbols (with error bars) for polycrystalline UO_2 samples prepared and analyzed by CEA; orange diamond and gray diamond for new experiments at CRL on polycrystalline and single-crystal UO_2 samples respectively. Diffusion coefficients derived from in-reactor measurements of iodine release from UO_2 single crystals (blue symbols [6]) are also shown for comparison. A solid orange circle depicts an additional data point for a measurement at 1700 °C that was made after the manuscript had been submitted (see text).

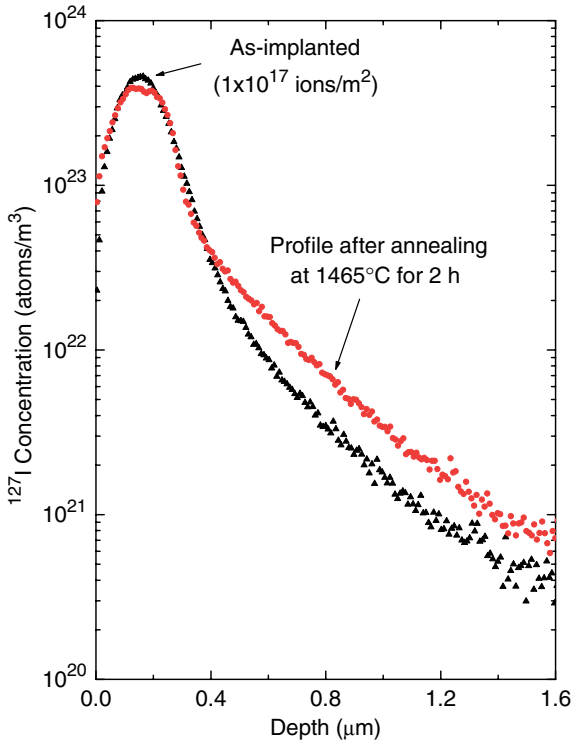

Fig. 10. Depth profiles of ^{127}I as-implanted in a UO_2 single-crystal at 930 keV to a fluence of 1×10^{17} ions/m^2 and after a thermal anneal at 1465 °C for 2 h under reducing conditions (sample prepared and analyzed at CRL).

3.2. Effects of stoichiometry on the solubility and diffusion of iodine in UO_{2+x}

Previous studies of polycrystalline UO_2 that had been ion-implanted with iodine to higher fluences (10^{17} or 10^{19} ions/m^2) revealed only limited evidence of thermal diffusion, even after annealing at high-temperatures (up to 1650 °C) for extended periods (up to 24 h) under reducing conditions [24]. These results were interpreted in terms of iodine trapping at relatively immobile defect sites, likely intragranular particles or bubbles in the nanometre size range. An illustrative example of the effects of thermal annealing at 1465 °C for 2 h on the distribution of iodine ion-implanted in a UO_2 single-crystal at 930 keV to a fluence of 1×10^{17} ions/m^2 is presented in Fig. 10. Aside from a slight decrease in the maximum iodine concentration, there has been negligible change in the iodine distribution over the peak of the profile. Conversely, diffusive spreading in the tail of the distribution below 3×10^{22} atoms/m^3 is comparable with that observed for polycrystalline UO_2 and consistent with the estimated threshold concentration for iodine trapping [24]. A threshold of ~10^{22} fissions/m^3 has also been found for trapping of xenon during post-irradiation thermal anneals of trace-irradiated fuel samples [15,17].

During irradiation of fuel within a reactor, the impact of trapping on the mobility of fission products with low solubility in the fuel matrix can be largely mitigated through re-solution caused by thermal spikes and displacement cascades associated with energetic fission fragments [13,14]. Although radiation damage can also directly enhance diffusion rates (RED) below ~1300 °C through creation of excess lattice vacancies, the vacancy population is maintained near equilibrium at higher temperatures [6,8]. The lowest energy site for both iodine and xenon atoms in the UO_2 lattice is a uranium vacancy combined with one or two oxygen vacancies, and a second adjacent uranium lattice vacancy is thought to be required for a single-step migration event [34–36]. Furthermore, the population of uranium lattice vacancies increases rapidly as a function of the degree of hyperstoichiometry [11,12]. Because the combined average valence of the fission products is slightly less than four (plutonium fission is more oxidizing than uranium fission), an incremental excess of oxygen can develop within the fuel matrix as a function of extended burnup [1,37], whereas any failure of the sheath would lead to significant oxidation of the fuel [1–3].

The impact of thermal annealing at 1400 °C for 2.5 h under slightly oxidizing conditions, sufficient to produce $UO_{2.02}$, on the distribution of iodine ion-implanted into polycrystalline UO_2 at 440 keV to a fluence of 1×10^{17} ions/m^2 is illustrated in Fig. 11. Duplicate profiles recorded from the as-implanted reference as well as the annealed and oxidized sample demonstrate excellent reproducibility. Pronounced migration of iodine into the bulk matrix has clearly been achieved here over the entire implanted-ion distribution. The maximum concentration at the peak of the as-implanted reference profile in Fig. 11 ($\sim 8 \times 10^{23}$ atoms/m^3) is well above the threshold level identified for defect trapping of iodine in stoichiometric UO_2 [24,30]. A good fit to the altered distribution over the entire profile was achieved with a constant diffusion coefficient of 2×10^{-17} m^2/s, which is two orders of magnitude greater than the narrow range of values determined for diffusion of iodine in stoichiometric UO_2 at 1400 °C (above). This also suggests that even a very slight departure from optimum conditions during the 1180 °C anneal could explain the larger than expected diffusion coefficient derived from the data in Fig. 1.

A thermodynamic model of the defect structure of the fluorite lattice predicts equilibria between the various types of defects (oxygen interstitials, uranium lattice vacancies, etc.) [12]. The fraction of uranium lattice sites that are vacant in UO_{2+x} can then be directly related to the degree of hyperstoichiometry by the following expression:

$$V_U = x^2 \cdot \exp[-(\Delta G_S - 2\Delta G_{FO})/kT], \quad (4)$$

where ΔG_S is the free energy of formation for a Schottky trio (a neutral trivacancy consisting of one uranium vacancy and two oxygen vacancies), ΔG_{FO} is the free energy of formation for an anti-Frenkel defect (an oxygen vacancy plus an oxygen interstitial), k is the Boltzmann constant and T is the absolute temperature. Thermodynamic data taken from the literature ($\Delta G_S = 6.3$ eV and $\Delta G_{FO} = 3.0$ eV) [33,38,39] were used to calculate V_U for the conditions of the experiment in Fig. 11 ($x = 0.02$ and $T = 1673$ K). The absolute number density of uranium lattice vacancies, N_{VU}, could then be estimated (from $N_{VU} = V_U \cdot N_U$ where N_U is the number density of uranium atoms in UO_2) to be about 10^{24} vac/m^3, which is just above the peak concentration of the as-implanted iodine distribution in Fig. 11. A similar calculation for pure, stoichiometric UO_2 (without implanted iodine) yielded a much smaller concentration of uranium lattice vacancies at 1400 °C ($N_{VU} \sim 10^{19}$ vac/m^3) [12].

The effects of thermal annealing at 1400 °C for 2.5 h under slightly oxidizing conditions, sufficient to produce $UO_{2.02}$, on the depth distribution of iodine ion-implanted into polycrystalline UO_2 at 440 keV to a fluence of 1×10^{19} ions/m^2 revealed much less diffusive spreading of iodine than was observed for the lower fluence case above (Fig. 11). Instead, trapping effects predominated over the peak of the distribution consistent with the fact that the solubility limit for iodine in $UO_{2.02}$ estimated above had been exceeded by two orders of magnitude.

Thermal diffusion of iodine, ion-implanted into polycrystalline UO_2 at 440 keV to a fluence of 1×10^{17} ions/m^2, at 1200 °C for 2.5 h under slightly oxidizing conditions, sufficient to produce $UO_{2.01}$, is illustrated in Fig. 12. Duplicate profiles recorded from the as-implanted reference as well as the annealed and oxidized sample again show excellent reproducibility. Diffusive spreading of the iodine is less pronounced here than was observed after the 1400 °C anneal of an equivalent sample oxidized to $UO_{2.02}$ (compare Figs. 11 and 12). Furthermore, there are some indications of trapping effects over the peak of the distribution, which suggests that the solubility limit was just exceeded at the maximum iodine concentration. This would be consistent with the fact that the number density of uranium lattice vacancies estimated using Eq. (4) for the present conditions (1200 °C and $x = 0.01$) is about a factor of five smaller than the value derived above ($\sim 10^{24}$ vac/m^3 for 1400 °C and $x = 0.02$). An approximate fit to the backside of the profile yielded a diffusion coefficient of 3×10^{-18} m^2/s, which is two orders of magnitude greater than the value determined for stoichiometric UO_2 at 1200 °C.

Because the diffusion rate of oxygen through the UO_{2+x} lattice is many orders of magnitude faster than that of iodine [12,16,17], the stoichiometry within the shallow layer containing the implanted-ion distribution should remain

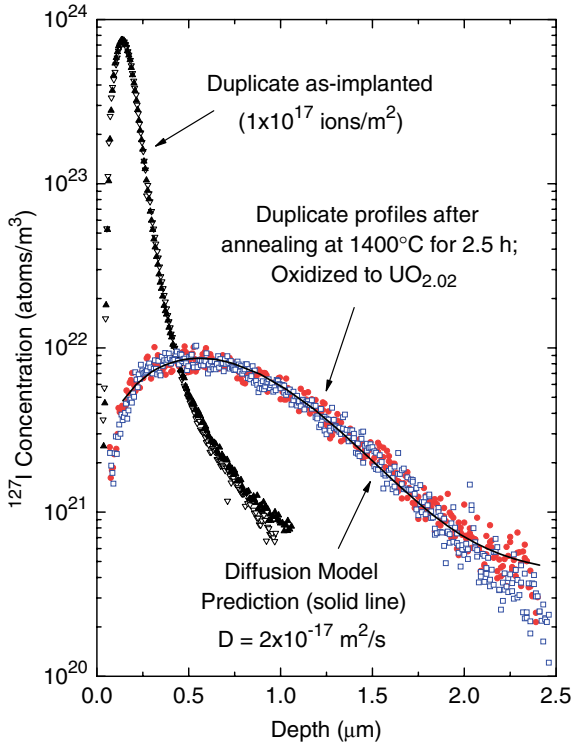

Fig. 11. Depth profiles of ^{127}I as-implanted into polycrystalline UO_2 at 440 keV to a fluence of 1×10^{17} ions/m^2 and after a thermal anneal at 1400 °C for 2.5 h under slightly oxidizing conditions sufficient to produce $UO_{2.02}$ (sample prepared and analyzed at CRL). The calculated (model prediction) distribution is indicated by the solid line.

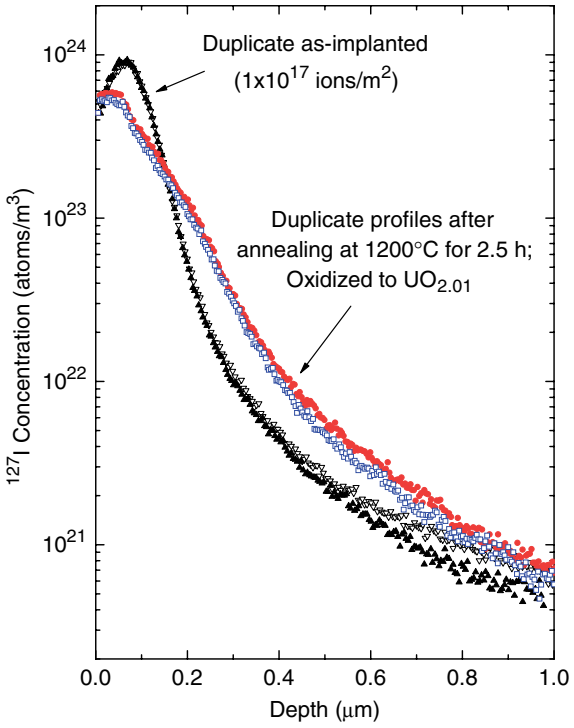

Fig. 12. Depth profiles of ^{127}I as-implanted into polycrystalline UO_2 at 440 keV to a fluence of 1×10^{17} ions/m^2 and after a thermal anneal at 1200 °C for 2.5 h under slightly oxidizing conditions sufficient to produce $UO_{2.01}$ (sample prepared and analyzed at CRL).

uniform throughout the anneal at peak temperature. However, there could be some increase in the O/U ratio over the isothermal stage as well as during the initial upward ramp, if the kinetics for reaction of oxygen at the surface are sufficiently slow [40]. Further evaluation of the oxidation process is warranted, which could lead to refinement of the coulometric-titration strategy to optimize this experiment.

4. Conclusions

An inter-laboratory comparison has provided enhanced confidence in the ion-implantation/SIMS method for investigating the migration behaviour of fission products in oxide nuclear fuels. New measurements of iodine diffusion in stoichiometric uranium dioxide – using different thermal annealing furnaces, different SIMS instruments and different analytical strategies – have yielded internally consistent results that are also in reasonable agreement with several previous experiments. A refined Arrhenius relationship for iodine thermal diffusion in stoichiometric UO_2 has been derived from a best fit to fourteen independent measurements spanning the temperature range 1200 °C to 1650 °C.

The combination of coulometric titration and ion-implantation/SIMS analysis has been shown to offer great potential for quantitatively determining the impact of hyperstoichiometry on iodine migration in fuel. Pronounced changes in iodine solubility as a function of the population of uranium lattice vacancies are clearly as important as enhanced thermal diffusion rates for influencing overall mobility and segregation tendency. This approach should also be readily applicable to a number of other fission products for which there is limited information on either solubility or diffusion in oxide fuels.

Acknowledgements

The authors would like to thank W.N. Lennard and J. Hendriks at the University of Western Ontario for ion implanting the samples that were annealed at CRL and C. Peaucelle of the Institut de Physique Nucléaire de Lyon for implanting samples that were annealed at CEA Cadarache. They are also grateful to Louis Raimbault of the CIG in Fontainebleau (France) for providing access to the SIMS equipment with which the group from CEA Cadarache carried out many of the analyzes.

References

[1] H. Kleykamp, J. Nucl. Mater. 131 (1985) 221.
[2] J.R. Matthews, J. Chem. Soc. Faraday Trans. 2 83 (1987) 1273.
[3] J.H. Gittus, J.R. Matthews, P.E. Potter, J. Nucl. Mater. 166 (1989) 132.
[4] L.H. Johnson, D.W. Shoesmith, in: W. Lutze, R.C. Ewing (Eds.), Radioactive Waste Forms for the Future, Elsevier Science, Amsterdam, 1988, p. 635, Chapter 11.
[5] B. Cox, J. Nucl. Mater. 172 (1990) 249.
[6] J.A. Turnbull, C.A. Friskney, J.R. Findlay, F.A. Johnson, A.J. Walter, J. Nucl. Mater. 107 (1982) 168.
[7] Hj. Matzke, Radiat. Eff. 64 (1982) 3.
[8] H. Wollenberger, V. Naundorf, M.P. Macht, in: R.P. Agarwala (Ed.), Diffusion Processes in Nuclear Materials, Elsevier, Amsterdam, 1992, p. 201.
[9] M. Hirai, J.H. Davies, R. Williamson, J. Nucl. Mater. 226 (1995) 238.
[10] R. Lindner, Hj. Matzke, Z. Naturforsch. 14a (1959) 582.
[11] J.C. Killen, J.A. Turnbull, in: K.A. Simpson, P. Wood (Eds.), Proceedings of a Workshop on Chemical Reactivity of Oxide Fuel and Fission Product Release, vol. 2, Berkeley Nuclear Laboratories, UK, 1987, p. 387.
[12] Hj. Matzke, Adv. Ceram. 17 (1986) 1.
[13] J.A. Turnbull, R.M. Cornell, J. Nucl. Mater. 41 (1971) 156.
[14] H. Blank, Hj. Matzke, Radiat. Eff. 17 (1973) 57.
[15] Hj. Matzke, Radiat. Eff. 53 (1980) 219.
[16] Hj. Matzke, J. Chem. Soc. Faraday Trans. 2 83 (1987) 1121.
[17] Hj. Matzke, in: R.P. Agarwala (Ed.), Diffusion Processes in Nuclear Materials, Elsevier, Amsterdam, 1992, p. 9.
[18] M.A. Mansouri, D.R. Olander, J. Nucl. Mater. 254 (1998) 22.
[19] W.H. Hocking, R.A. Verrall, P.G. Lucuta, Hj. Matzke, Radiat. Eff. Def. Solids 125 (1993) 299.
[20] A.H. Booth, A method of calculating fission gas diffusion from UO_2 fuel and its application to the X-2-f loop test, Atomic Energy of Canada Limited Report, CRDC-721/AECL-496, 1957.
[21] S.G. Prussin, D.R. Olander, W.K. Lau, L. Hansson, J. Nucl. Mater. 154 (1988) 25.
[22] A.C.S. Sabioni, W.B. Ferraz, F. Millot, J. Nucl. Mater. 257 (1998) 180.
[23] W.H. Hocking, R.A. Verrall, S.J. Bushby, in: International Atomic Energy Agency Technical Committee Meeting Proceedings, IAEA-TECDOC-1122, 1999, p. 111.
[24] W.H. Hocking, R.A. Verrall, I.J. Muir, J. Nucl. Mater. 294 (2001) 45.
[25] Hj. Matzke, A. Turos, J. Nucl. Mater. 114 (1983) 349.

[26] R.A. Verrall, J.F. Mouris, Z. He, in: D.B. Sanderson (Ed.), Proceedings of the 8th International Conference on CANDU Fuel, Canadian Nuclear Society, Honey Harbour, Ontario, 2003, p. 65.
[27] L. Desgranges, B. Pasquet, Nucl. Instrum. and Meth. B 215 (2004) 545.
[28] R.G. Wilson, F.A. Stevie, C.W. Magee, Secondary Ion Mass Spectrometry: A Practical Handbook for Depth Profiling and Bulk Impurity Analysis, Wiley, New York, 1989.
[29] J.F. Ziegler, J.P. Biersack, U. Littmark, The Stopping and Range of Ions in Solids, Pergamon, New York, 1985, and SRIM Code at <www.SRIM.org>.
[30] M. Saidy, R.A. Verrall, J.F. Mouris, I.J. Muir, W.H. Hocking, in: D.B. Sanderson (Ed.), Proceedings of the 8th International Conference on CANDU Fuel, Canadian Nuclear Society, Honey Harbour, Ontario, 2003, p. 137.
[31] M. Saidy, J.F. Mouris, W.H. Hocking, R.A. Verrall, in: F.C. Iglesias (Ed.), Proceedings of the 9th International Conference on CANDU Fuel, Canadian Nuclear Society, Belleville, Ontario, 2005, Paper B4002 and Atomic Energy of Canada Limited Report, CW-124600-CONF-001.
[32] H.S. Carlslaw, J.C. Jaeger, Conduction of Heat in Solids, Second ed., Clarendon, Oxford, 1959.
[33] Hj. Matzke, in: O.T. Sorensen (Ed.), Nonstoichiometric Oxides, Academic, New York, 1981, p. 155, Chapter 4.
[34] C.R.A. Catlow, Proc. Royal Soc. London A 364 (1978) 473.
[35] R.G.J. Ball, R.W. Grimes, J. Chem. Soc. Faraday Trans. 86 (1990) 1257.
[36] G. Busker, R.W. Grimes, M.R. Bradford, J. Nucl. Mater. 279 (2000) 46.
[37] W.H. Hocking, F.J. Szostak, in: R. Sejnoha (Ed.), Proceedings of the 6th International Conference on CANDU Fuel, Canadian Nuclear Society, Niagara Falls, Ontario, 1999, p. 127.
[38] Hj. Matzke, J. Nucl. Mater. 30 (1969) 26.
[39] Hj. Matzke, in: H. Blank, R. Lindner (Eds.), Proceedings of the 5th International Conference on Plutonium and Other Actinides, North-Holland, Amsterdam, 1976, p. 801.
[40] J. Abrefah, A. de Aguiar Braid, W. Wang, Y. Khalil, D.R. Olander, J. Nucl. Mater. 208 (1994) 98.